

Spectroscopic Analysis of a Pulsed-Laser Deposition System for Fullerene-like C_{n_x} Film Production

H. Riascos · G. Zambrano · P. Prieto

Received: 22 September 2005 / Accepted: 9 January 2006 /

Published online: 14 April 2006

© Springer Science+Business Media, Inc. 2006

Abstract Plasma produced by a (1064 nm) Nd:YAG laser focused onto a graphite target at different nitrogen pressures in the range of 1–90 mTorr, was studied spectroscopically. In the spectral range of 350–600 nm, emission lines of CI neutral carbon (501.12, and 505.21 nm), NI neutral nitrogen (493.5 nm), CII (426.72, 463.7, 515.11 nm), and CIII ions (465.02 and 569.59 nm), and NII ions (501.06, and 500.73 nm), were dominating. Bands of C_2 Swan ($d^3\Pi_g \rightarrow a^3\Pi_u$, $\Delta v = 2, 1, 0, -1$), and CN Violet ($B^2\Sigma^+ \rightarrow X^2\Sigma^+$, $\Delta v = 1, 0, -1$) systems, and ionic emissions from the First Negative system N_2^+ (band head at 391.44 nm), were faintly observed under our specific experimental conditions. From the band intensities, vibrational temperature for CN and C_2 was calculated to be 1.25 and 0.31 eV at 90 mTorr, respectively. The electron density and temperature, measured by Stark broadening, assuming a local thermodynamic equilibrium (LTE), were found to be $2.1 \times 10^{17} \text{ cm}^{-3}$ and 0.33 eV at 1 mTorr, respectively. The validity of the LTE is discussed according to the results discussed. Pressure dependence shows a decrease in the vibrational temperature when nitrogen pressure increases, while the electron density and temperature increase.

Keywords Optical emission spectroscopy · Laser ablation · Plasma properties · Fullerene related materials

PACS 61.48.+c · 52.38.Mf · 52.25-b · 52.70. Kz · 78.30.-j · 81.05.Tp

1. Introduction

The characterization of laser-ablation plasmas through the determination of their main parameters, as temperature, electron density, and number densities of the different species present in the plasma, has gained high interest in recent years, allowing to improve the process control

H. Riascos

Departamento de Física, Universidad Tecnológica de Pereira, A. A. 097, Pereira, Colombia

G. Zambrano · P. Prieto (✉)

Excellence Center for Novel Materials, Departamento de Física, Universidad del Valle,

A. A. 25360, Cali, Colombia

E-mail: pprieto@calima.univalle.edu.co

and providing better understanding of these complex and versatile spectroscopic sources. Temperature is a crucial parameter that, if local thermodynamic equilibrium (LTE) is satisfied, determines the distribution of level excitation through the Boltzmann equation and the ionization equilibrium through the Saha equation. For LTE existence in plasma, electron density has to be high enough so that collisional rates exceed radiative rates. In this case, the so-called excitation (Boltzmann) and ionization (Saha) temperatures coincide with the electronic temperature, i.e., with the temperature of the Maxwellian distribution of electron velocities [1].

The most widely used method to determine the temperature of laser-ablation plasmas has been the Boltzmann plot method, which provides the excitation temperature from the measurement of line emissions from a single species. In its simplest form, only two emission lines, which differ on their upper level energies, are necessary to obtain the excitation temperature [2, 3]. In some works, Boltzmann plots have been obtained from a higher number of emission lines [3–8]; in this case, a good correlation of the experimental data to a linear fitting indicates the validity of the Boltzmann equation. In some cases, the measured line intensities corresponded to the emission from the whole plasma [3, 4], so the Boltzmann plot method provided a single value of the excitation temperature of the plasma. Also, time resolution is used in light detection, as the plasma temperature is known to experience a rapid decrease due to the plasma expansion. In other cases, the emission from the plasma is spatially resolved in order to obtain the temperature at a given distance from the sample [6, 8].

A second method used in some works [9–12] to obtain the plasma temperature is based on the Saha equation that relates the number densities of consecutive ionization stages of an element in combination with the Boltzmann equation, yielding the population distribution for each species. In this method, the ionization temperature is obtained from the emission lines of the neutral atom and the ion of an element. The advantage of this method with respect to the Boltzmann plot method is that a wider range of upper-level energies may be obtained by including lines from neutral atoms and ions, which results in higher accuracy in the resulting temperature values. Ionization temperature was obtained, in some cases, from the emission intensity of the whole plasma [10] and, in other cases, with spatial resolution in the axial direction [11, 12]. In some works, the Saha–Boltzmann method was applied using two lines, one from the neutral atom and another from the ion [10–12].

Pulsed-laser deposition (PLD) has been broadly used to grow a variety of carbon-containing refractory films such as diamond-like carbon [13–15], carbon nitride [16–18] and, silicon carbide [19, 20]. In particular, since the theoretical study by Liu and Cohen [21], extensive work has been done to deposit β -phase carbon nitride known as superhard material by laser ablation of a graphite target in a nitrogen atmosphere.

In PLD, the properties of the film growth are mostly affected by laser-ablation plasma, the so-called “plume” produced by irradiation of a target using a high-power laser pulse. The plume consists of target materials, which are to be transferred to a substrate mounted facing the target. The composition of the plume is nearly identical to that of the target although there could be some mismatch due to incongruent melting of the target and/or intentional supply of atoms from the ambient gas. For instance, inclusion of nitrogen atoms is achieved by supplying nitrogen via reactive laser ablation of a graphite target in a nitrogen atmosphere.

Not only do such quantitative properties, but also dynamic properties like kinetic energy of each species in the plume have significant effects upon the PLD-grown films. Additionally, vibrational and rotational temperatures of the molecules produced by chemical reactions in the plume are expected to be important parameters in determining plume properties. In this respect, it would be important to elucidate the correlation between plasma parameters

and deposited film properties [22, 23], one of the ultimate goals of the research on PLD mechanisms.

In this work, we present experimental results on the laser ablation of a graphite target in nitrogen atmosphere, calculating the velocity of plume expansion and formation of molecules by using the optical emission spectroscopy method. Optical emissions from the excited C_2 and CN molecules, as well as atomic species — both ionic and neutral — were observed and the vibrational temperatures of C_2 and CN molecules in their electronically excited states and electron and ionization temperature were derived.

Evolution of the carbon plasma-plume generated by laser ablation of a graphite target in a reactive gas is strongly dependent upon ablation conditions such as laser wavelength, fluence, ambient gas, and pressure. Particularly, the evolution of C_2 and CN molecules in the plume were reported to be directly affected by ambient gas pressure. However, the expansion and formation mechanisms of C_2 and CN molecules are as of yet not fully understood, demanding further investigation.

2. Experimental setup

The experimental setup and experimental procedure were described previously [17, 24]. We used a short-pulse, Q-switched Nd: YAG laser which provided 7-ns, 500-mJ laser pulses at a wavelength of 1064 nm with a 10-Hz repetition rate. The experiment took place in a stainless steel vacuum chamber configured as a six-way cross of 10 cm inner diameter tubes forming a central 10-cm diameter target chamber evacuated to 10^{-5} mTorr, and flushed with pure nitrogen (99.999) at different flow rates during experiments. The laser beam was focused with a 20-cm focal length lens on a graphite target (99.99%) with a 45° angle of incidence, giving an energy density of approximately 10 J/cm^2 . Nitrogen gas (99.999%) was injected to the chamber as a reactive gas, and the flow of such was accurately controlled by a needle valve. During laser ablation, nitrogen pressure was varied from 1 to 90 mTorr as measured by a vacuum gauge. The substrate was placed at a distance of 30 mm from the target. The films were deposited on silicon substrates that had previously been ultrasonically cleaned in acetone.

Emission spectra were collected, imaged onto spectrograph TRIAX 550™ with 1200 grooves/mm grating and a resolution of 0.025 nm using two 10 and 13 cm focal length lenses positioned outside the reactor. For time-integrated spectra measurements, the spectrograph was equipped with a CCD linear sensor (1024×256). Most of the spectra were collected with integration times of 1 s.

3. Results and discussion

Figure 1 displays the emission spectra, taken at a distance of approximately of 1 cm from the target, over a range from 350 to 600 nm at a fluence of 10 J/cm^2 at a wavelength of 1064 nm and 7 ns energy pulse from different nitrogen pressures. The observed spectra contain a large number of peaks, causing notable superposition, and making identification of various band heads difficult. Identification of atomic and molecular species was made by comparing observed spectral lines with the files of known lines [25–27], reported in Table 1. Major peaks are labeled, corresponding to the specie producing the spectral peaks. Highly emissive species include neutral and ionized atomic carbon (CI, CII and CIII), diatomic

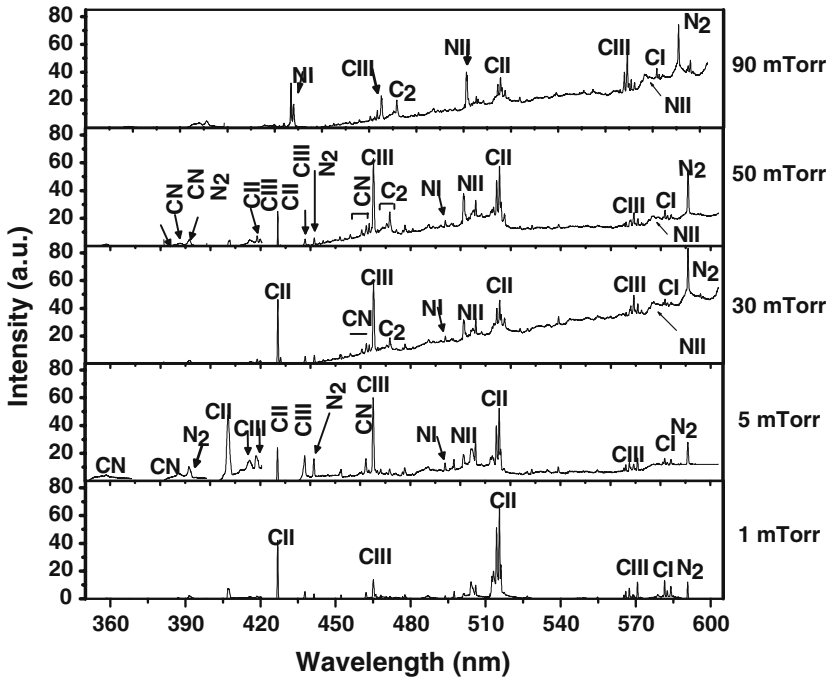


Fig. 1 Typical time-integrated optical emission spectra during laser ablation of graphite at different nitrogen pressures. Laser fluence was set at $10\text{J}/\text{cm}^2$

nitrogen and carbon, and CN. The spectra were also characterized by a strong continuum emission, originating from different transition mechanisms involving free electrons.

As seen in Fig. 1 in the spectral range from 350 to 600 nm, emission lines of CI neutral carbon (501.12 and 505.21 nm), NI neutral nitrogen (493.5 nm), CII (426.72, 463.7, 515.11 nm), and CIII ions (465.02 and 569.59 nm), and NII ions (501.06 and 500.73 nm), were dominated. Bands of C_2 Swan ($d^3\Pi_g \rightarrow a^3\Pi_u$, $\Delta\nu = 2, 1, 0, -1$), and CN Violet ($B^2\Sigma^+ \rightarrow X^2\Sigma^+$, $\Delta\nu = 1, 0, -1$) systems, and ionic emissions from the First Negative system N_2^+ (band head at 391.44 nm), were faintly observed under our specific experimental conditions. In addition, intense line of first positive of N_2 (590.6 nm) was observed. Emission intensities were highly dependent on nitrogen pressures [22, 28].

The general structure of the spectra does not vary much with the N_2 pressure, while the intensities of the specific emissions do (see Fig. 1). CII and CIII lines varied in emission intensities as nitrogen pressure increased from 1 to 90 mTorr, but no clear trend was observed. The intensities of bands of CN Violet ($\Delta\nu = 2$) and C_2 Swan ($\Delta\nu = 1$) systems slightly increase in this pressure range; and at 1 mTorr their intensities are quite weak. Although for ionic emissions from N_2^+ (band head at 391.44 nm) their intensities are very low, this band head increases when nitrogen pressure increases. However, background emission intensities increased with the increase in nitrogen pressure. It should be noted that emission intensities of the first positive of N_2 (590.6 nm) system increased drastically with nitrogen pressure. As reported, the expansion of the plume is limited at high pressures and the plume is spatially confined [23, 29]. Consequently, dissociation rates of CN molecules overtake formation rates at high pressures given the increased number of energetic collisions in the plume.

Table 1 Identification of atomic and molecular species observed during graphite ablation in nitrogen gas at 10 J/cm^2 with a 7-ns energy pulse.

Wavelength (nm)	Specie	Transition		Wavelength (nm)	Specie	Transition	
		Electronic	Vibrational			Electronic	Vibrational
358.39	CN	$B^2\Sigma \rightarrow X^2\Sigma$	$v' = 3, v'' = 2$	493.21	Cl	$1P^* - 1S$	
358.59	CN	$B^2\Sigma \rightarrow X^2\Sigma$	$v' = 2, v'' = 1$	500.39	N_2	$A^2\Pi \rightarrow X^2\Sigma$	$v' = 14, v'' = 6$
385.47	CN	$B^2\Sigma \rightarrow X^2\Sigma$	$v' = 3, v'' = 3$	501.01	N_2	$A^2\Pi \rightarrow X^2\Sigma$	$v' = 18, v'' = 9$
387.14	CN	$B^2\Sigma \rightarrow X^2\Sigma$	$v' = 1, v'' = 1$	501.27	N_2	$B^2\Sigma^+ \rightarrow X^2\Sigma_g^+$	$v' = 3, v'' = 6$
391.44	N_2	$B^2\Sigma_u^+ \rightarrow X^2\Sigma_g^+$	$v' = 0, v'' = 0$	502.38	Cl		
406.89	CIII	$5g\ ^3G \rightarrow 4f^3F^0$		502.49	Cl		
407.59	CII			503.59	CII		
415.24	CN	$B^2\Sigma \rightarrow X^2\Sigma$	$v' = 5, v'' = 6$	504.35	N_2	$A^2\Pi \rightarrow X^2\Sigma$	$v' = 10, v'' = 3$
415.67	CIII	$5f\ ^3G \rightarrow 3p\ ^3F^0$		505.36	N_2	$B^3\Pi_g^+ \rightarrow A^3\Sigma_u^+$	$v' = 11, v'' = 5$
415.81	CN	$B^2\Sigma \rightarrow X^2\Sigma$	$v' = 4, v'' = 5$	512.93	C_2	$A^3\Pi_g \rightarrow X^3\Pi_u$	$v' = 1, v'' = 1$
418.1	CN	$B^2\Sigma \rightarrow X^2\Sigma$	$v' = 2, v'' = 3$	513.32	CII	$4P^* - 4P$	
419.72	CN	$B^2\Sigma \rightarrow X^2\Sigma$	$v' = 1, v'' = 2$	514.51	CII	$4P^* - 4P$	
423.65	N_2	$C^2\Sigma_u^+ \rightarrow X^2\Sigma_g^+$	$v' = 1, v'' = 2$	515.10	CII	$4P^* - 4P$	
426.73	CII	$2D - 2F^*$		516.52	C_2	$A^3\Pi_g \rightarrow X^3\Pi_u$	$v' = 0, v'' = 0$
427.81	N_2	$C^2\Sigma_u^+ \rightarrow X^2\Sigma_g^+$	$v' = 0, v'' = 1$	517.58	CIII	$1P^* - 1D$	
437.95	CIII	$3D - 3P^*$		557.36	CIII	$3P^* - 3S$	
441.65	N_2	$C^3\Sigma_u \rightarrow B^3\Sigma_g$	$v' = 3, v'' = 8$	554.59	CIII	$3D - 3P^*$	

Table 1 continued

Wavelength (nm)	Specie	Transition		Wavelength (nm)	Specie	Transition		Vibrational
		Electronic	Vibrational			Electronic	Vibrational	
450.22	CN	$B^2\Sigma \rightarrow X^2\Sigma$	$v' = 5, v'' = 7$	535.4	N ₂	$A^2\Pi \rightarrow X^2\Sigma$	$v' = 8, v'' = 2$	
451.48	CN	$B^2\Sigma \rightarrow X^2\Sigma$	$v' = 4, v'' = 6$	537.28	N ₂	$B^3\Pi_g^+ \rightarrow A^3\Sigma_u^+$	$v' = 12, v'' = 7$	
451.68	CIII	3D – 3P*		538.03	Cl	1P* – 1P		
453.19	CN	$B^2\Sigma \rightarrow X^2\Sigma$	$v' = 3, v'' = 5$	554.72	Cl	3D – 3P*		
455.41	N ₂	$B^2\Sigma_u^+ \rightarrow X^2\Sigma_g^+$	$v' = 3, v'' = 5$	560.37	Cl	3S – 3P*		
460.61	CN	$B^2\Sigma \rightarrow X^2\Sigma$	$v' = 0, v'' = 2$	564.8	CII	4P* – 4S		
462.7	Cl	3P – 1S		565.31	N ₂	$B^2\Sigma_u^+ \rightarrow X^2\Sigma_g^+$	$v' = 2, v'' = 6$	
463.76	CII	2P* – 2D		566.24	CII	4P* – 4S		
465.02	CIII	3S – 3P*		569.59	CIII	1P* – 1D		
467.86	C ₂	$A^3\Pi_g \rightarrow X^3\Pi_u$	$v' = 5, v'' = 4$	572.99	N ₂	$A^2\Pi \rightarrow X^2\Sigma$	$v' = 6, v'' = 1$	
468.5	C ₂	$A^3\Pi_g \rightarrow X^3\Pi_u$	$v' = 4, v'' = 3$	578.49	Cl	3P – 3P*		
477.17	Cl	3P* – 3P		581.77	Cl	3P – 3P*		
477.6	Cl	3P* – 3P		582.64	CIII	1D – 1F*		
481.29	Cl	3P* – 3S		590.6	N ₂	$B^3\Pi_g^+ \rightarrow A^3\Sigma_u^+$	$v' = 9, v'' = 5$	
491.68	N ₂	$C^3\Sigma_u \rightarrow B^3\Sigma_g$	$v' = 1, v'' = 7$	595.9	N ₂	$B^3\Pi_g^+ \rightarrow A^3\Sigma_u^+$	$v' = 8, v'' = 4$	
				596.93	Cl	3D* – 3D		

For CN_x growth, a direct reaction of molecular nitrogen with carbon is a non-probable process [30], hence atomic nitrogen generation in the CN radical formation is necessary.

3.1. Determination of vibrational temperature

For plasma in local thermodynamic equilibrium (LTE), the number densities at various vibrational levels of the molecule in the excited state can be evaluated using the Boltzmann distribution [31–35].

$$\ln \sum_{v''} (\lambda^4 I_{v'v''}) = C - G(v') \frac{hc}{kT_{\text{vib}}} \quad (1)$$

where λ is the wavelength corresponding to the emission, h Planck's constant, c the velocity of light, C a constant, $G(v')$ the term value corresponding to the vibrational level in the upper electronic state and T_{vib} the vibrational temperature. Determination of the vibrational temperature, T_V , requires the analysis of several vibrational bands that belong to a given electronic transition and differ in the vibrational quantum numbers, v' (upper vibrational level) and v'' (lower vibrational level).

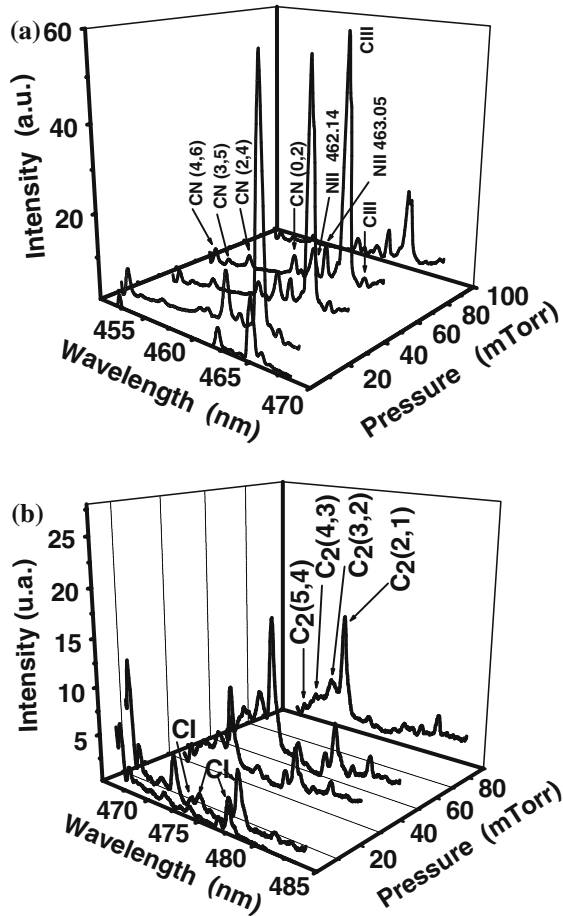
Figure 2 shows the CN Violet ($B^2\Sigma^+ - X^2\Sigma^+$, $\Delta v = 2$) and C_2 Swan ($A^3\Pi_g - X'^3\Pi_u$, $\Delta v = 1$) systems in which some peaks are labeled on the plot. Moreover, the effects of gas pressure on emission intensities of C_2 and CN molecules are illustrated in Fig. 2. In these spectra, very intense CI and CII emission lines overlap some bands of these sequences.

To avoid measurement errors associated with spectral overlap, the CN Violet ($B^2\Sigma^+ - X^2\Sigma^+$, $\Delta v = 2$) and C_2 Swan ($A^3\Pi_g - X'^3\Pi_u$, $\Delta v = 1$) sequences of these systems are used to calculate the vibrational temperature.

The vibrational temperatures for bands C_2 Swan ($\Delta v = 1$, in the 467–474 nm range) and CN Violet ($\Delta v = 2$, in the 450–460 nm range) systems respectively, were obtained from a plot of the sums of the band-head strengths measured in various v' or v'' progressions against the vibrational term values $G(v')$. The spectroscopic constants $G(v')$ used for the calculations were obtained from Handbook [36].

CN Violet and C_2 Swan vibrational temperatures were determined at different nitrogen pressures. Calculation of vibrational temperatures for violet system using Boltzmann distribution of graphite ablation with fluence of 10 J/cm^2 at different nitrogen pressures is shown in Fig. 3. The dependence of the vibrational temperatures of CN molecules on gas pressure is given in Fig. 4. It can be seen that the increase in nitrogen pressure decreased the vibrational temperatures of the CN species from 1 to 90 mTorr ranges. This is probably because the nitrogen atmosphere cooled the hot electrons as well as excited states of molecules by collisions leading to a more efficient thermalization; thereby decreasing the vibrational temperature. This result also implies that the distribution of vibrationally excited states was not in equilibrium with the plasma at low pressures. The addition of nitrogen and hence the increase of the pressure, improved the confinement of the plasma, which in turn enhanced the emission from molecular and atomic nitrogen species. This is also supported by the enhancement observed in the intensities of C_2 bands on increasing the nitrogen pressure, as seen in Fig. 2. The C_2 vibrational temperature decreases with gas pressure increase. However, in Fig. 4 we observe that the CN temperature is higher than for C_2 . In general, it is believed that CN molecules are formed by energetic collisions of C_2 and N_2 , while C_2 molecules are mostly generated by the recombination of carbon atoms with a non-activation barrier in the gas phase [37, 38]. This explains why CN molecules are vibrationally much hotter than C_2 as shown in Fig. 4.

Fig. 2 Time-integrated spectrum of laser plasma plume; (a) Evolution spectrum with gas pressure reveals some bands of the CN violet system $\Delta v = 2$; (b) Evolution spectrum with gas pressure reveals some bands of the swan system $\Delta v = 1$. Both cases show the effects of gas pressure upon line intensities



For CN molecules at 90 mTorr of nitrogen pressure, the vibrational temperature was 1.25 eV. These values agree with values previously reported using laser [32–35, 39–41] and other techniques [42, 43].

3.2. Determination of electron temperature

Assuming LTE resulting from collisions in the plasma, the populations of the bound states follow the Boltzmann distribution. The relative line intensities from a particular state can be used to calculate the electron temperature of the plasma [44, 45].

$$\ln \left(\frac{I_{mn} \lambda_{mn}}{A_{mn} g_{mn}} \right) = \ln \left(\frac{N}{Z} \right) - \left(\frac{E_m}{\kappa T_e} \right) \quad (2)$$

where λ_{mn} is the transition wavelength, I_{mn} the intensity of the observed transition line, A_{mn} the transition probability, g_{mn} degeneracy of the upper level, E_m the energy of the upper level, κ the Boltzmann constant, N the total number of states, Z the partition function, and T_e the electron temperature. For the transition, the upper state is labeled as m and the lower state by n . The slope $(-1/\kappa T_e)$ of the plot of $\ln(I_{mn} \lambda_{mn}/A_{mn} g_{mn})$ versus E_m yields temperature.

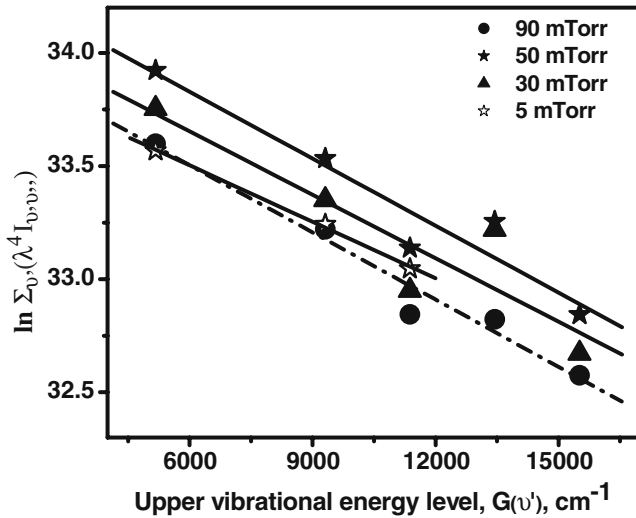
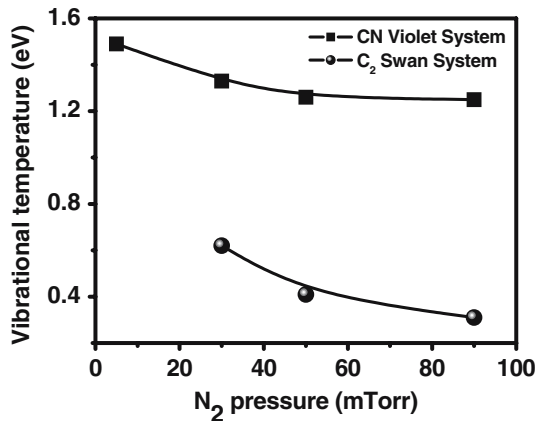


Fig. 3 Calculation of vibrational temperatures for violet system using Boltzmann distribution of graphite ablation with fluence of 10 J/cm^2 at different nitrogen pressures

Fig. 4 Vibrational temperatures determined from optical emission spectra of C_2 and CN molecules at different nitrogen pressures. Laser fluence was set at 10 J/cm^2

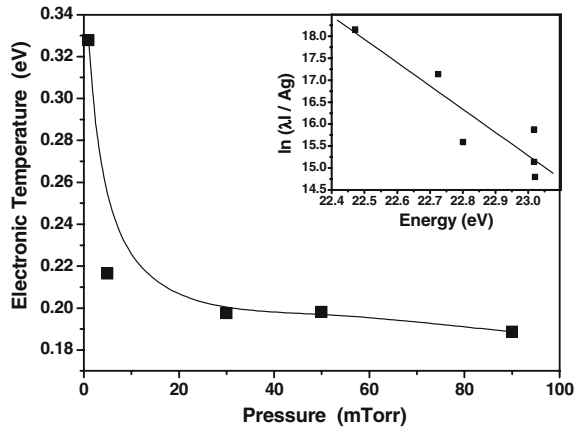


The spectroscopic lines whose transition probabilities [16] and the other parameters are known were taken from the recorded spectra at different gas pressures.

We obtained temperatures near 0.33 eV at nitrogen pressures of 1 mTorr at laser fluence of 10 J/cm^2 using the 463.7, 512.52, 513.29, 514.52 nm, and 515.11 nm CII lines. Figure 5 shows that electron temperature at various pressures decreases slightly with nitrogen pressure. The inset in Fig. 5 shows the Boltzmann plot used to estimate T_e at 90 mTorr. Electron temperature determinations are jeopardized given the overlapping effect.

The CN vibrational temperature is about three times higher than the electron temperature, which is typical for a nonequilibrium vibrational distribution [1, 46]. In general, we observed higher electron and vibrational temperatures for lower gas pressure, since in-vacuum plasma expands freely while the ambient gas confines it to a smaller region resulting in reduced expansion rates and hence an enhanced cooling rate due to collisions. The rate at

Fig. 5 Electronic temperature at $10\text{J}/\text{cm}^2$ determined by using Equation 2 at various nitrogen pressures. Inset: Boltzmann plot at 90 mTorr



which temperature changes depends on elastic collisions, electron heating—due to collisional de-excitation of metastable ions, along with recombination effects [1, 46].

3.3. Estimation of electron density

There are three possible broadening mechanisms that can occur in the laser-ablated plume. The Doppler broadening, resulting from motion of the atoms, the Stark-broadening from collisions with charged species, and the resonance broadening arising from collisions between the neutral species exciting strong resonance lines [1, 45]. Estimation of electron density depends principally upon the measurement of the Stark and Doppler broadening of some optical lines [45]. Doppler broadening is estimated by using the formula $(\Delta\lambda)_{1/2} = 7.16 \times 10^{-7} \lambda (T_e/M)^{1/2}$, where T_e is the electron temperature in Kelvin and M the atomic mass [47]. In our case, for the $3d^2D-4f^2F^0$ transition of singly ionized carbon (CII) at 426.7 nm with $T_e = 3801\text{ K}$ (0.33 eV) at 1 mTorr, the Doppler line width is 0.0054 nm; much less than the 0.30 nm full width at half maximum (FWHM) observed in our experiment, so the effect due to Doppler broadening can be ignored. Stark broadening of an isolated line in the plasma was, thus, used to estimate electron density in the plasma. The $3s^2P-4p^2S^0$ transition of atomic nitrogen (NI) at 493.5 nm was used for electron density measurements. The Stark-broadened profiles were recorded at various pressures and fitted to the Lorentzian profile.

FWHM $(\Delta\lambda)_{1/2}$ of the Stark-broadened of a line, is related to the electron density through the expression [44, 47]

$$\Delta\lambda_{1/2} = 2W \left(\frac{n_e}{10^{16}} \right) + 3.5A \left(\frac{n_e}{10^{16}} \right)^{1/4} \times \left(1 - \frac{3}{4} N_D^{-1/3} \right) W \left(\frac{n_e}{10^{16}} \right) \quad (3)$$

It is the sum of two (electron impact and ion-impact) terms. A is the ion broadening parameter and W is the electron impact-width parameter. Both W and A are nearly temperature independent [45]. N_D is the number of particles in Debye sphere at a plasma temperature and T_e is given by

$$N_D = \frac{1.72 \times 10^9 [T_e(\text{eV})]^{3/2}}{[n_e(\text{cm}^{-3})]^{1/2}} \quad (4)$$

The contribution is almost entirely due to electron impact, and the half-width of the Stark-broadened transition can be estimated by the first term in Equation (3) to a good approximation [48]. Expression (3) reduces to

$$\Delta\lambda_{1/2} = 2W \left(\frac{n_e}{10^{16}} \right) \tag{5}$$

where n_e is the electron density in cm^{-3} . The line shapes observed were corrected by subtracting the contribution of the instrumental width at its minimum 0.025 nm using

$$\Delta\lambda_{\text{true}} = \Delta\lambda_{\text{observed}} - \Delta\lambda_{\text{instrumental}} \tag{6}$$

The W and A parameters can be found in Ref. [45]. Figure 6 shows the variation of electron density as a function of nitrogen pressure for a plume produced at a laser fluence of $10\text{J}/\text{cm}^2$. The inset in Fig. 6 shows a typical broadened profile, FWHM of 0.37 nm, fitted with a Lorentzian line obtained at 1 mTorr of nitrogen gas and $10\text{J}/\text{cm}^2$. Using typical values from our experiment, we found particle density in Debye sphere $\text{ND} = 0.5$. Using broadening parameters ($W = 0.00806\text{ nm}$ and $A = 0.0044\text{ nm}$) the line width due to ionic contribution is estimated to be 0.04 nm, much less than the observed width in our experiments.

To estimate the number density of two consecutive ionization stages for locally equilibrated plasma, we used Saha equation [49]:

$$\frac{n_i n_e}{n_a} = 2 \frac{Z_i}{Z} \left(\frac{2m\kappa T_e}{h^2} \right)^{3/2} \exp \left(-\frac{E_i}{\kappa T_e} \right) \tag{7}$$

where n_i , n_e , and n_a are the number density of singly charged ions, electrons and neutral atoms, respectively, Z_i , Z are partition functions of the ion and the atom, and E_i is the ionization potential. For nitrogen plasma the equation (7) can be rewritten as:

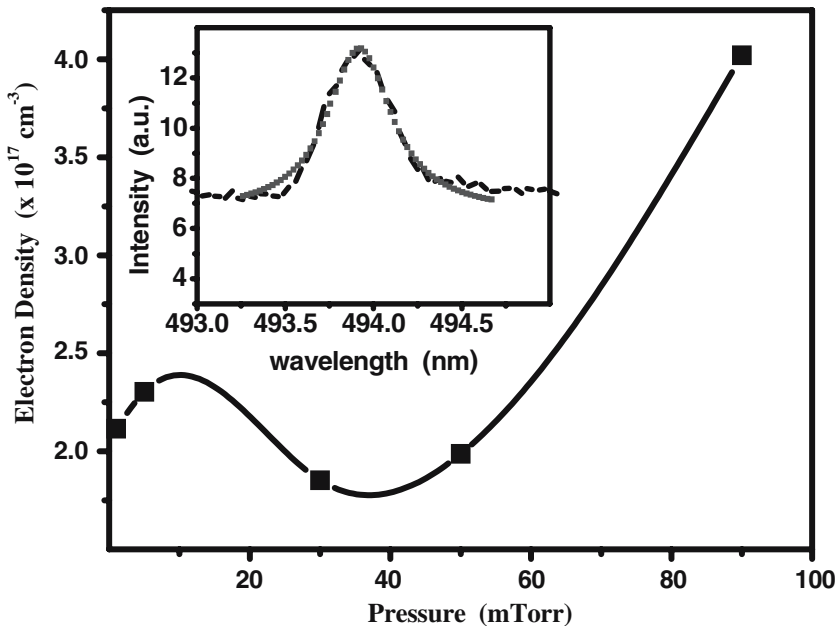


Fig. 6 Variation of plasma electron density (n_e), calculated from Stark broadening, at a laser fluence of $10\text{J}/\text{cm}^2$. Inset: Stark-broadened profile for NI transition ($3s^2P-4p^2S^0$) at 493.51 nm. Dotted line represents the Lorentzian fit

$$\frac{n_i}{n_a} = \frac{2.04 \times 10^{15}}{n_e} (\kappa T_e)^{3/2} \exp\left(-\frac{11.26}{\kappa T_e}\right) \quad (8)$$

Using the measured values of electron temperature, we found that the fractional ionization is low for different pressures, for $T_e = 0.33$ eV and densities of about $2.3 \times 10^{17} \text{ cm}^{-3}$. The fractional ionization is around 3×10^{-12} ; the degree of ionization remains low until E_i is only a few times lower than T_e [50], suggesting that the recombination rate, in this region, is very high and therefore we have weakly ionized plume plasma, given that the electronic temperature is lower than ionization potential of the species. In practice, the heating of the plasmas occurs at temperatures above 1 eV (over the boiling points of most materials) by inverse-Bremsstrahlung absorption of the laser light in a free. Free transition of an electron-ion pair; the absorption coefficient for this process better predicts absorption at longer laser wavelengths; however, it requires higher densities in the order of 10^{19} cm^{-3} for significant absorption. For pulsed-laser deposition (PLD) processes, these conditions are normally not fulfilled [50, 51].

3.4. Local thermodynamic equilibrium (LTE)

Since for our analysis of T_e we have assumed plasma is in LTE, it is worth to check in these experiments the conditions for LTE. In a transient system, such as the plume formed by a pulsed-laser beam, for LTE to be fulfilled, the electron–atom and electron–ion collision processes must be extremely rapid and must dominate the radiative processes [44, 45]. In a system at LTE, particles will have Maxwellian velocity distributions, populations of the species in their energy levels will follow Boltzmann statistics, and the ionization processes will be described by Saha's equation and radiation density will obey Planck's law.

Clearly, for LTE the electron density must be sufficiently high. Befeki [45] and McWhirter [49] has derived a necessary (but not sufficient) criteria for LTE

$$n_e \geq 1.4 \times 10^{14} T_e^{12} (\Delta E_{mn})^3 \text{ cm}^{-3}, \quad (9)$$

where T_e is the electron temperature in eV, and ΔE_{mn} is the energy difference between the upper and lower energy levels (in eV). Substituting values for T_e (0.38 eV) and ΔE (2.51 eV) in (9) the lowest limit for n_e is $1.37 \times 10^{15} \text{ cm}^{-3}$. Our calculated values of n_e are two orders of magnitude higher than this limit, implying that LTE approximation for these analyses is valid.

The velocity of the plasma was also analyzed. Whenever the LTE criteria are satisfied, the velocity of the plasma produced by Nd: YAG laser in nitrogen gas is given by [52]:

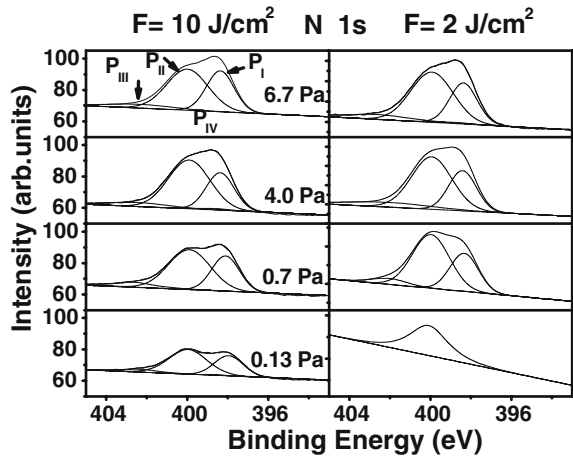
$$v = \left(\frac{2}{\gamma - 1}\right) \left(\frac{\gamma \kappa T_e}{M}\right)^{1/2} \quad (10)$$

where M is the mass species and γ is defined as the ratio of specific heat for the plume. In the current case where the laser fluence is 10 J/cm^2 , $T = 0.33$ eV at 1 mTorr, and the specific heat ratio of the diatomic molecule vapor $\gamma = 1.4$, plasma velocity is found to be $6.5 \times 10^5 \text{ cm/s}$, reasonably agreeing with previous work [53].

3.5. CN_x film characterization

Carbon Nitride (CN_x) thin films were deposited on silicon (100) and (111) substrates at a temperature of 300°C by PLD technique at 2 and 10 J/cm^2 at a gas pressure of 1–90 mTorr [24]. The composition and structural properties of the as-deposited films were investigated as functions of gas pressure. X-ray photoelectron spectroscopy (XPS) revealed a

Fig. 7 XPS N1s core level spectra of CN_x thin films deposited by PLD of graphite at indicated pressures and fluence



strong dependence of the amount of structurally incorporated nitrogen upon the gas pressure, where a maximum was observed at the highest laser fluence of 10 J/cm^2 and an intermediate pressure of 30 mTorr. Further analyses of the XPS N1s core level spectra of the CN_x films, exhibiting the highest elasticity in nano-indentation experiments, revealed a typical double peak arrangement, which is most pronounced for the highest laser fluence at low pressures. These two peak components indicate that the nitrogen bonded into a graphitic structure dominates over the twofold coordinated pyridine-like bonding configuration. This favors the growth of intersecting corrugated graphene structures that may be considered to have a “fullerene-like” microstructure. The N1s and C1s XPS spectra of the CN_x films show two major binding energy bands centered at about 400 eV and at about 285 eV, respectively. These bands are characteristic for the bonding structure of nitrogen and carbon. The evolution of the N1s level spectra of carbon nitride films deposited at different pressures at a laser fluence of 2 and 10 J/cm^2 is reported in a previous work [24] and, we also discussed on the interpretation the peak contribution in N1s XPS peak (Fig. 7).

Peaks I and II are main components, Peak I on 398–399 eV (PI) is related to twofold coordinated sp^2 -hybridized nitrogen (sp^2 C–N) bonds — attributed to electrons originating from nitrogen atoms having two neighbors just like in Pyridine. Nitrogen atoms can also be bonded substitutional for carbon in a graphite ring system. Peak II on 400.0–400.8 eV (PII) corresponds to the respective sp^2 C–N bonds, originating from nitrogen atoms having three neighbors [24, 54]. The ratio of peaks I and II separated by approximately 2 eV, can be taken as an indicator that the microstructure of the films is fullerene-like, if the ratio of P_{II}/P_I is greater than 1 [55, 56]. As seen in Fig. 8, there is a clear decrease in the P_{II}/P_I peak ratio with an increase in gas pressure, we observe similar trends in vibrational and electron temperature of plasma (Figs. 4 and 5).

According to Voevodin [57] et al. the availability of CN radicals with a high vibrational temperature was suggested to promote the formation of fullerene-like CN_x in laser ablation of graphite targets at low nitrogen pressures.

4. Conclusions

We used the optical emission spectroscopy method to analyze the chemical species generated by the Nd:YAG pulsed-laser irradiation of nanosecond duration of a graphite target in a

nitrogen atmosphere. C_2 and CN molecules were the dominant sources of optical emission at pressures above 90 mTorr. At low pressures below 50 mTorr, CI, CII and CIII were the most enriched species in the plume. Vibrational temperatures of electronically excited C_2 and CN molecules were obtained by Boltzmann plot method of the experimental spectra. CN molecules were hotter than C_2 molecules; presumably given the differences in their formation mechanisms: C_2 molecules are formed by a recombination of carbon atoms, while CN molecules are produced through a chemical reaction between C_2 and N_2 .

Electron temperature and plasma density change with increases in nitrogen pressure. The LTE approximation is valid for these generated plumes, where the Stark effect is the principal mechanism for line broadening. The Saha–Eggert equation is applied to calculate the degree of ionization in the vapor phase, on the basis of the assumption that local thermal equilibrium is reached.

Acknowledgments This work was supported by *COLCIENCIAS*, under the 1106-05-11457 research project, the Excellence Center for Novel Materials under contract 043-2005, and by the *Fundación para la Promoción de la Investigación y la Tecnología del Banco de la República*, under the 1441 research project.

References

1. Griem HR (1977) Principles of plasma spectroscopy, Cambridge University Press, Cambridge
2. Narayanan V, Thareja RK (2004) Appl Surf Sci 222:382
3. Joseph MR, Xu N, Majidi V (1994) Spectrochim Acta B 49:89
4. Sattmann R, Sturm V, Noll R (1995) J Phys D Appl Phys 28:2181
5. Lee Y.-I, Sneddon J (1996) Spectrosc Lett 29:1157
6. Hermann J, Thomann AL, Boulmer-Leborgne C, Dubreuil B, De Giorgi M, Perrone A, Luches A, Mihăilescu IN (1995) J Appl Phys 77:2928
7. Castle BC, Visser K, Smith BW, Winefordner JD (1997) Acta B 52:1955
8. Aguilera JA, Aragón C (2004) Spectrochim Acta B 59:1861
9. Keszler AM, Nemes L (2004) J Mol Struct 695–696:211
10. Milán M, Laserna JJ (2001) Spectrochim Acta B 56:275
11. Harilal SS, Bindhu CV, Isaac RC, Nampoori VPN, Vallabhan CPG (1997) J Appl Phys 82:2140
12. Harilal SS, Bindhu CV, Nampoori VPN, Vallabhan CPG (1998) Appl Spectrosc 52:449
13. Witanachi S, Miyawa AM, Mukherjee P (2000) Mat Res Soc Symp 617 J3–6:2
14. Wei Q, Narayan RJ, Sharma AK, Sankar J, Narayan JJ (1999) Vac Sci Technol, A 17:3406
15. Qian F, Singh RK, Dutta SK, Pronko PP (1995) Appl Phys Lett 67:3120
16. Pan WJ, Sun J, Ling H, Xu N, Ying ZF, Wu JD (2003) Appl Surf Sci 218:297
17. Riascos H, Zambrano G, Prieto P, Arroyave M, Devia A, Galindo H (2004) Surf Coat Tech 188–189:617
18. Acquaviva S, Caricato AP, De Giorgi ML, Luches A, Perrone A (1997) Appl Surf Sci 109–110:408
19. Neri F, Trusso S, Vasi C, Barreca F, Valisa P (1998) Thin Solid Films 332:290
20. Leggieri G, Luches A, Martino M, Perrone A, Alexandrescu R, Barborica A, Gyorgy E, Mihăilescu IN, Majani G, Mengucci P (1996) Appl Surf Sci 96–98:866
21. Liu AY, Cohen ML (1989) Science 245:841
22. Yamagata Y, Sharma A, Narayan J, Mayo RM, Newman JW, Ebihara K (1999) J Appl Phys 86:4154
23. Aldea E, Caricato AP, Dinescu G, Luches A, Perrone A (1997) Jpn. J Appl Phys 36:4686
24. Riascos H, Neidhardt J, Radnóczy GZ, Emmerlich J, Zambrano G, Hultman L, Prieto P (2005) Thin Sol. Films (to be published)
25. Striganov AR, Sventitskii NS (1968) Tables of spectral lines of neutral and ionized atoms, IFI Plenum, New York
26. Gaydon AP (1976) The identification of molecular spectra, Chapman and Hall, London
27. NIST Atomic Spectra Database, <http://physics.nist.gov>
28. Mao D, Tao K, Hopwood J (2002) J Vac Sci Technol A 20(2):379
29. Harilal SS, Isaac RC, Bindhu CV, Gopinath P, Nampoori VPN, Vallabhan CPG (1997) Spectrochim Acta A 53:1527
30. Veprek S, Weidmann J, Glatz F (1995) J Vac Sci Technol A 13(6):2914
31. Riascos H, Zambrano G, Prieto P (2004) Brazilian J Phys 34(4B):1583
32. Voevodin AA, Jones JG, Zabinski JS (2002) J Appl Phys 92:724

33. Yamagata Y, Sharma A, Narayan J, Mayo RM, Newman JW, Ebihara K (1999) *J Appl Phys* 86:4154
34. Harilal SS, Issac RC, Bindhu CV, Nampoori VPN, Vallabhan CPG (1997) *J Phys D* 30:1703
35. Chen X, Mazumder J, Purohit A (1991) *Appl Phys A: Solids Surf* 52:328
36. CRC Handbook of chemistry and physics, 84th ed. 2003–2004.
37. Park SM, Chae H, Wee S, Lee IJ (1998) *Chem Phys* 109:928
38. Bae CH, Park SM (2002) *J Chem Phys* 117:5347
39. Park HS, Nam SH, Park SM (2004) *Bull Korean Chem Soc* 25:5
40. Yamagata Y, Sharma A, Narayan J, Mayo RM, Newman JW, Ebihara K (2000) *J Appl Phys* 88:6861
41. Bulir J, Novotny M, Jelinek M, Jastrabik L, Zelinger Z (2003) *Surf Coat Tech* 173–174:968
42. Laux CO, Spence TG, Kruger CH, Zare RN (2003) *Plasma Sources Sci Technol* 12:125
43. Zelinger Z, Novotny M, Bulir J, Kubát P, Jelinek M (2003) *Contrib. Plasma Phys* 43(7):416
44. Griem HR (1964) *Plasma spectroscopy*, McGraw-Hill, New York
45. Bekefi G (1976) *Principles of laser plasmas*, Wiley-Interscience, New York
46. Cacciatore M, Capitelli M, De Benedictis S, Dilonardo M, Gorse D (1986) *Nonequilibrium vibrational kinetics*, Springer-Verlag, Berlin
47. Wiese WL (1965) In: Huddleston RH, Leonard SL (eds) *Plasma diagnostics techniques*, Academic, New York
48. Khare A, Thareja RK (1988) *IEEE J Quant Electr* 24:2525
49. McWhirter RWP (1965) In: Huddleston RH, Leonard SL (eds) *Plasma Diagnostics Techniques* Leonard Academic, New York
50. Chen FF (1974), *Introduction to plasma physics*, Ch. 1, Plenum, New York
51. Ashfold MNR, Claeysens F, Fuge GM, Henley SJ (2004) *Chem Soc Rev* 33:23
52. Chrisey DB, Hubler GK, (1994) *Pulsed laser deposition of thin films*, Ch. 5, Wiley New York
53. Pietch W (1996) *J Appl Phys* 79:1250
54. Hellgren N, Guo J, Sätze C, Agui A, Nordgren J, Luo Y, Ågren H, Sundgren J-E (2001) *Appl Phys Lett* 76:4348
55. Neidhardt J, Hultman L, Czigány Zs (2004) *Carbon* 42:2729
56. Voevodin AA, Jones JG, Zabinski JS, Czigány Zs, Hultman L (2002) *J Appl Phys* 92(9):724
57. Voevodin AA, Jones JG, Zabinski JS, Hultman L (2000) *J Appl Phys* 92(9):4980